Groundwater

High-Resolution Integrated Transport Model for Studying Surface Water–Groundwater Interaction

by Tabea Broecker[1,2], Vahid Sobhi Gollo[1], Aryeh Fox[3], Jörg Lewandowski[4,5], Gunnar Nützmann[4,5], Shai Arnon[3], and Reinhard Hinkelmann[1]

Abstract

Transport processes that lead to exchange of mass between surface water and groundwater play a significant role for the ecological functioning of aquatic systems, for hydrological processes and for biogeochemical transformations. In this study, we present a novel integral modeling approach for flow and transport at the sediment–water interface. The model allows us to simultaneously simulate turbulent surface and subsurface flow and transport with the same conceptual approach. For this purpose, a conservative transport equation was implemented to an existing approach that uses an extended version of the Navier–Stokes equations. Based on previous flume studies which investigated the spreading of a dye tracer under neutral, losing and gaining flow conditions the new solver is validated. Tracer distributions of the experiments are in close agreement with the simulations. The simulated flow paths are significantly affected by in- and outflowing groundwater flow. The highest velocities within the sediment are found for losing condition, which leads to shorter residence times compared to neutral and gaining conditions. The largest extent of the hyporheic exchange flow is observed under neutral condition. The new solver can be used for further examinations of cases that are not suitable for the conventional coupled models, for example, if Reynolds numbers are larger than 10. Moreover, results gained with the integral solver provide high-resolution information on pressure and velocity distributions at the rippled streambed, which can be used to improve flow predictions. This includes the extent of hyporheic exchange under varying ambient groundwater flow conditions.

Introduction

Stream water can enter the streambed, mix with groundwater and return after traveling some distance to the overlying water body. The zone of the streambed where at least 10% of the pore water is stream water is called "hyporheic zone" (Harvey and Bencala 1993). The hyporheic zone plays a fundamental role for the transport and transformation of pollutants and natural solutes as well as habitat and refugium for aquatic organisms (Sophocleous 2002; Boulton et al. 2010; Hester and Gooseff 2010; Krause et al. 2013; Lewandowski et al. 2019). Hyporheic exchange can be generated by streambed morphologies such as meanders, bars, ripples, or other obstacles (Bencala and Walters 1983; Elliott and Brooks 1997; Packman et al. 2004; Tonina and Buffington 2007; Cardenas 2009). The exchange depends on the sediment permeability and head gradients (Dent et al. 2007; Buffington and Tonina 2009; Cardenas 2009; Ruehl et al. 2009; Bardini et al. 2012; Wu et al. 2018). Solutes are exchanged with groundwater and stream water, too. Thereby, contaminants can

[1]Chair of Water Resources Management and Modeling of Hydrosystems, Technische Universität Berlin, Berlin, Germany; vahid.sobhigollo@tu-berlin.de; reinhard.hinkelmann@wahyd.tu-berlin.de

[2]Corresponding author: Chair of Water Resources Management and Modeling of Hydrosystems, Technische Universität Berlin, Gustav-Meyer-Allee 25, 13355 Berlin, Germany; 0049 30 314 72308; fax: 0049 30 314 72430; tabea.broecker@uwi.tu-berlin.de

[3]Department of Environmental Hydrology and Microbiology, Zuckerberg Institute for Water Research, The Jacob Blaustein Institutes for Desert Research, Ben-Gurion University of the Negev, Sede Boqer Campus, Israel; aryehfoxxx@gmail.com; sarnon@bgu.ac.il

[4]Ecohydrology Department, Leibniz-Institute of Freshwater Ecology and Inland Fisheries, Berlin, Germany; lewe@igb-berlin.de; nuetzmann@igb-berlin.de

[5]Geography Department, Humboldt-University Berlin, Berlin, Germany; lewe@igb-berlin.de; nuetzmann@igb-berlin.de

Article Impact Statement: A novel integral high-resolution model is used to simulate flow and transport processes at the groundwater surface water interaction space.

Received August 2020, accepted December 2020.

doi: 10.1111/gwat.13071

be transported from surface water to groundwater and vice versa (van der Molen et al. 1998; Lewandowski et al. 2011b; Engelhardt et al. 2014). As a result, on the one hand a spreading of contamination is possible; on the other hand the water quality can also be improved, for example, by nutrient turnover or the retention and/or transformation of trace organic compounds in the hyporheic zone (Brunke and Gonser 1997; Heberer et al. 2008; Botter et al. 2010; Huntscha et al. 2012; Lawrence et al. 2013; Regnery et al. 2015; Schaper et al. 2018; Schaper et al. 2019). Important parameters for the solute exchange and biogeochemical reactions within the hyporheic zone are hyporheic exchange flux, residence times within the sediment, and the biogeochemical milieu (Zarnetske et al. 2011; Bardini et al. 2012; Gomez et al. 2012; Marzadri et al. 2012; Arnon et al. 2013; Trauth et al. 2015).

Due to increasing interest on hyporheic zones, many studies rely on field and laboratory experiments and investigated the magnitude and direction of water exchange (Kasahara and Wondzell 2003; Peterson and Sickbert 2006; Gariglio et al. 2013; Lewandowski et al. 2019). While for real case observations of hyporheic exchange processes, field studies are preferred, detailed process understanding and generalizations are more difficult to derive from such studies. Compared to field studies, flumes studies allow to control various factors such as permeability, water levels, or discharges. For a deeper understanding of physical principles of the complex dynamics at the sediment–water interface, modeling studies have the advantage to contribute a high-resolution process understanding, both spatially and temporally. This is particularly important for groundwater, where measurements providing high spatial resolution are challenging. Moreover, information about variables that are difficult to measure such as turnover rates can be determined with modeling approaches. However, especially for the validation of these models, experimental data are still needed.

Numerical simulations of flow in the hyporheic zone usually couple a surface water flow model to a flow model of the porous sediment—considering different time scales. Often, a one-way sequential coupling method is applied, where pressure distributions from the surface water are used as a boundary condition for the groundwater model with no feedback from groundwater to surface water (Cardenas and Wilson 2007b, 2007c; Jin et al. 2011; Trauth et al. 2013; Trauth et al. 2014). But also, some coupled models with feedback from the subsurface to the surface and vice versa (e.g., Nützmann and Mey [2007]) and fully coupled models such as the integrated hydrology model (VanderKwaak 1999) or HydroGeoSphere have already been applied for the exchange of groundwater and surface water (Brunner et al. 2009; Brunner and Simmons 2012; Alaghmand et al. 2014). For these models the two-dimensional diffusion-wave approximation of the St. Venant equations is applied for surface water and the three-dimensional Richards equation is used for the subsurface. To simultaneously solve one system of equations, exchange flux terms are applied in these models. Li et al. (2020) presented a fully coupled model for the hyporheic zone using Open Source Field Operation and Manipulation (OpenFOAM). The Navier–Stokes equations used for surface water are coupled with the Darcy equation by flux boundary conditions at the interface through an iterative algorithm. In the present study, an extended version of the three-dimensional Navier–Stokes equations is used for the whole system. The integral solver for surface water and groundwater was developed by Oxtoby et al. (2013) and was already validated and applied for the hyporheic zone in Broecker et al. (2019). The solver allows to investigate feedbacks from surface to subsurface and vice versa directly with one time step in the whole domain and is applicable also in non-Darcy-flow areas with Reynolds numbers higher than 10 (Broecker et al. 2019).

The impact of gaining and losing flow conditions on hyporheic exchange was previously simulated by Cardenas and Wilson (2007b, 2007c); Trauth et al. (2013), but only with one-way sequential coupled models with no feedback to surface water. Li et al. (2020) emphasized the necessity of fully coupled models and stated that for conservative solute transport in closed systems, the sequential model shows incorrect results. The difference between the results of one-way coupled and fully coupled models depends on permeability. Especially for increasing permeabilities, one-way sequential coupling is not sufficient (Li et al. 2020). To our knowledge, up to now there is no integral modeling approach that comprises turbulent flow and transport over and within dunes or ripples. Our integral model can also show turbulent effects that penetrate into the sediment, which is especially significant for bigger grain sizes. This penetration of turbulence into the sediment can directly control the interfacial exchange (Roche et al. 2018). Moreover, the feedback from groundwater to surface water can be important for intense up- or downward groundwater flow that affects the turbulent boundary layer (Prinos 1995; Cheng and Chiew 1998).

For the present study an additional transport equation is added to the existing integral modeling approach by Oxtoby et al. (2013) to investigate next to flow processes the transport of a conservative tracer. The correct description of the extended solver will be investigated with the help of flume experiments after Fox et al. (2014). Within these experiments, effects of neutral conditions (no in- or outflowing subsurface flow), outflowing subsurface flow (losing condition) and inflowing subsurface flow (gaining condition) on hyporheic exchange fluxes were analyzed with a laboratory flume system. We compare the simulated transport of a dye tracer with photographs taken during the experiments after Fox et al. (2014) and provide insights into flow processes at the rippled streambed for the conducted laboratory experiments with high-resolution results gained with the integral solver.

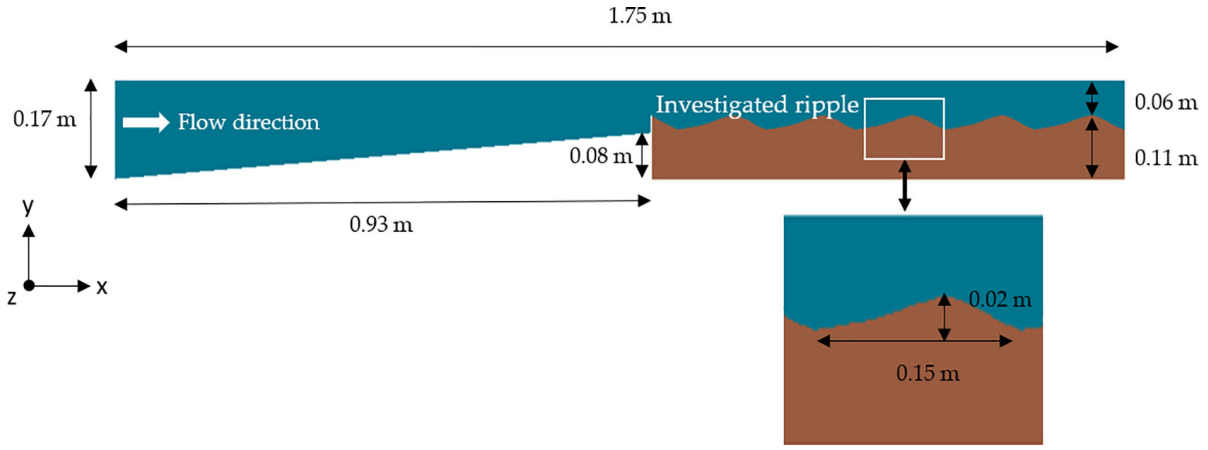

Figure 1. Model geometry for neutral conditions (sediment: brown, water: blue).

Materials and Methods

Geometry and Mesh

The geometry of the numerical model is based on the flume experiments of Fox et al. (2014). To reduce the computing time, the length of the 6.4 m long flume is shortened to approximately 1.75 m in the two-dimensional model. The shortened numerical model is a cut of the original flume. Only one phase which considers the surface water as well as the water in the sediment is taken into account. According to the water level used in the flume experiment the model has a height of 0.17 m. The dune-shaped sediment is located downstream of a ramp with a height of 0.08 m and a length of 0.93 m. The model geometry for the neutral case can be seen in Figure 1. For losing and gaining conditions the ripple geometries were adjusted slightly according to the photographs of the experiments. For this purpose, the meshes were modified manually. The average length of the bed form structures amounts to 15 cm, the height to 2 cm. The bed form geometry used in the experiments is commonly found in sandy streambeds (Stofleth et al. 2008; Lewandowski et al. 2011a; Harvey et al. 2013).

The mesh generator gmsh (Geuzaine and Remacle 2009) was used to discretize the two-dimensional mesh. About 77,000 unstructured elements were chosen to depict the dune shaped profiles. The exact number varies slightly for the different morphologies, while similar mesh conditions were chosen for the three meshes with similar element sizes in surface water, in the sediment and at the interface. Small element sizes at the interface of surface water and subsurface were used to account for the steep velocity gradients at the interface. The minimum element area of the applied mesh amounts to 1.93×10^{-7} m^2 and is located at the interface, while the maximum area amounts to 0.0033 m^2 and is located within the surface water.

Numerical Model

The open-source computational fluid dynamics (CFD) package OpenFOAM version 2.4.0 was used to simulate the dye spreading at the rippled streambed. The solver applied is based on the "porousInter" solver by Oxtoby et al. (2013). This solver uses the Navier–Stokes equations in surface water and in the sediment without any additional parameters. Solvers within the standard OpenFOAM library determining the interaction of surface water and groundwater—as porousInterFoam—apply resistance source terms for which such additional parameters as Darcy–Forchheimer coefficients are needed. For this reason, we decided to use the porousInter solver by Oxtoby et al. (2013). Since this solver only considers flow processes, we extended this solver for the investigation of transport processes. Flow processes are still determined using the equations available in the porousInter solver. PorousInter is based on the interFoam solver of OpenFOAM and is a multiphase solver for immiscible fluids (such as water and air) which extends the three-dimensional Navier–Stokes equations by the consideration of soil porosity and effective grain size diameter. All values represented by $[\ ]^f$ are averaged over the pore space volume. The equations for the conservation of mass and momentum are defined after Oxtoby et al. (2013):

Mass conservation

$$\varphi \nabla \cdot \left[\vec{\mathrm{U}}\right]^f = 0 \tag{1}$$

Momentum conservation

$$\varphi\left(\frac{\partial [\rho]^f \left[\vec{\mathrm{U}}\right]^f}{\partial t} + \left[\vec{\mathrm{U}}\right]^f \nabla \cdot \left([\rho]^f \left[\vec{\mathrm{U}}\right]^f\right)\right) = -\varphi \nabla \left[p\right]^f + \varphi [\mu]^f \nabla^2 \left[\vec{\mathrm{U}}\right]^f + \varphi [\rho]^f \vec{g} + \mathrm{D} \tag{2}$$

with φ representing the soil porosity (−); $\vec{\mathrm{U}}$ the velocity (m/s); ρ the density (kg/m^3); t the time (s); p the pressure (Pa); μ the dynamic viscosity (Ns/m^2), g the gravitational acceleration (m/s^2), and D as an additional drag term (kg/[m^{2}s^2]).

The drag term is defined after Oxtoby et al. (2013) to account for the momentum loss by means of fluid friction with the porous medium after Ergun (1952) and for flow

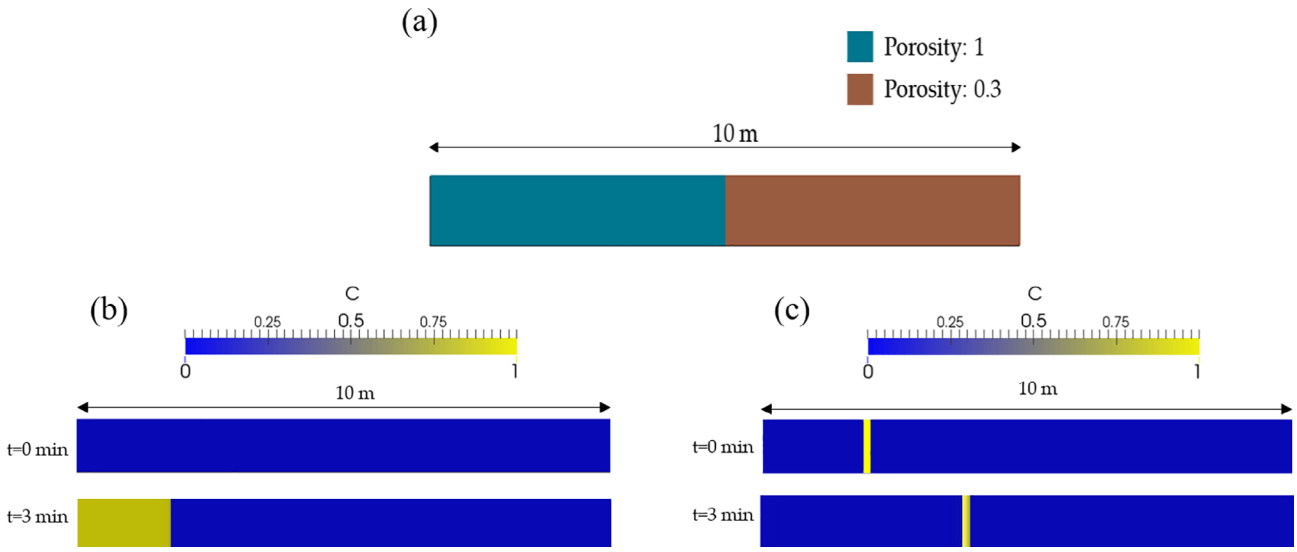

Figure 2. Model geometry (a) and tracer distribution at $t = 0$ min and at $t = 3$ min for a constant injection (b) and for a pulse injection (c).

recirculation after van Gent (1995):

$$D = -\left(150\frac{1-\varphi}{d_p\varphi}[\mu]^f + 1.75[\rho]^f\left[\vec{U}\right]^f\right)\frac{1-\varphi}{d_p}\left[\vec{U}\right]^f - 0.34\frac{1-\varphi}{\varphi}\frac{[\rho]^f\partial\left[\vec{U}\right]^f}{\partial t} \quad (3)$$

with d_p (m) as effective grain size diameter.

An advection–diffusion equation for a passive tracer with a concentration C was implemented into the porousInter-solver. According to Huettel et al. (2003), Jones and Mulholland (2000), Mermillod-Blondin et al. (2000), and Burnett et al. (2003), advection dominates at the sediment–water interface. This observation is consistent with our results and no dispersion in groundwater was included. Consequently, the only transport parameter for this approach is the molecular diffusion coefficient D_{mol} (m^2/s) and no calibration of transport parameters is needed. Due to the small cell sizes numerical diffusion is subordinate. The transport equation is defined as:

$$\frac{\partial C}{\partial t} + \nabla\cdot\left(C\vec{U}\right) + \nabla\cdot\left(D_{mol}\right)\nabla C = 0 \quad (4)$$

The standard k-epsilon turbulence model, which is based on the Reynolds averaged Navier–Stokes equations (RANS), is applied. Using the RANS turbulence model, not all scales of turbulence are directly resolved, instead they are modeled through different approaches. The turbulent flow is divided into an average and a fluctuating velocity and leads to a Reynolds stress tensor in the Navier–Stokes equations which is often computed with the help of two-equation models. Two extra transport equations represent the turbulent flow properties. Commonly, the transported variables are either k for turbulent kinetic energy and ε for the turbulent dissipation within the k-ε turbulence model or k and ω (specific dissipation) within the k-ω turbulence model. In contrast to more advanced turbulence models, such as Large Eddy Simulations (LES) or direct numerical simulations (DNS), much less computation time is needed for the RANS turbulence models. For DNS even the smallest turbulences are resolved, while for LES the large-scale eddies are resolved and the small-scale eddies are taken into account with a subgrid scale model. Already with the standard k-epsilon turbulence model, the computation time of 1-min simulation for the reduced two-dimensional geometry amounts to ~5 h on 100 parallel processors using the high-performance computing clusters of the Technische Universität Berlin with a MPP system. For LES, the cell sizes need to be decreased drastically and generally three, instead of two dimensions have to be considered. With the application of the RANS turbulence model an accurate description of tracer spreading is demonstrated compared to laboratory observations, which allows us to maintain the applied turbulence model with less computational effort.

Validation with One-Dimensional Analytical Results

Two different cases were used for a first validation of the implemented transport application of the integral solver. The simulated results were compared to analytical one-dimensional results for a continuous and for a pulse injection after Kinzelbach (1992). For the validation of the flow processes we refer to Broecker et al. (2019).

For the first case, a 10-m long one-dimensional domain was separated in two equal parts—the first half consists of water (porosity of 1), the second consists of soil with a porosity of 0.3 and an effective grain size diameter of 1 cm (Figure 2a). A conservative tracer with a molecular diffusion coefficient of 10^{-9} m^2/s flowed continuously into the water phase at the inlet (Figure 2b). The flow velocity at the inlet was fixed to 0.01 m/s. For

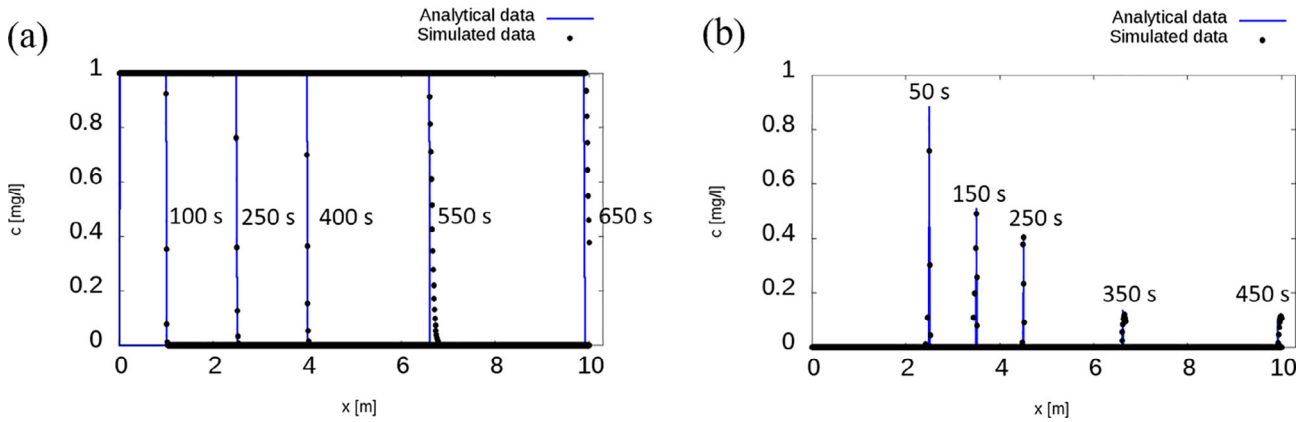

Figure 3. Comparison of simulated and analytically calculated concentrations for a constant injection (a) and for a pulse injection (b).

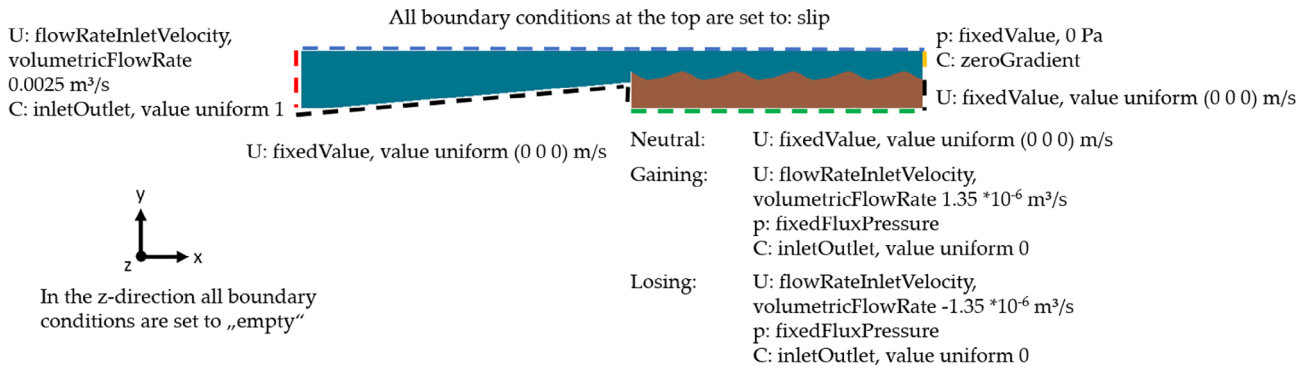

Figure 4. Boundary conditions (blue—overlying water; brown—sediment; U—velocity; C—tracer concentration; p—pressure; different colors of dashed lines indicate the different boundaries for the specified boundary conditions).

the second case, the setup was very similar, but instead of a continuous injection, a pulse injection was assumed. At the beginning, the tracer was placed into a line of 2 m to 2.01 m (Figure 2c). Afterwards, no further tracer injection was assumed and only the spreading of this tracer mass was observed.

The simulated tracer breakthrough curves for the constant and the pulse injection were compared with analytical results and showed a good agreement for the transport of a conservative tracer in surface water and the subsurface as it can be seen in Figure 3.

Boundary and Initial Conditions

The examined sandy sediment has a medium grain size of 0.384 mm and a porosity of 0.33. The most relevant boundary conditions can be seen in Figure 4. At the inlet, surface water enters the domain with a fixed discharge of 0.0025 m^3/s and a velocity of 0.0507 m/s. Because of the shallower depth of the water column above sediment the flow velocity on the right side of the domain shown in Figure 1 is higher. In Fox et al. (2014) the velocity of the surface water above the sediment was 0.123 m/s for a mean water level of 0.07 m and a flume width of 0.29 m. The spatial dimensions of our model domain are identical except for the reduced flume length. The discharge and the velocity at the inlet were calculated accordingly. All boundary conditions at the top contain slip conditions. We decided to apply a one-phase model to reduce the computational effort under the assumption that the water level fluctuations are negligible. Within the flume experiment, the water depth was kept constant also for losing and gaining conditions. All boundary conditions in the third dimension are set to "empty" which is a boundary condition implemented in OpenFOAM to describe sidewalls of two-dimensional geometries. At the left and at the right side of the sediment and at the ramp, walls with no-slip condition are defined. The wall at the right side of the sediment was also placed in the original flume, however not after 1.75 m, but after 6.4 m. Moreover, the original flume was recirculating while we defined the surface water to flow out of the domain. The outflowing discharge of the water equals the inflowing discharge. For the neutral conditions the bottom of the sediment is also a wall, while for the gaining and losing conditions the flux is fixed at the bottom of the sediment. The flowrates of $\pm 1.35 \times 10^{-6}$ m^3/s were calculated according to the inflow area at the bottom (0.29 m × 0.82 m) and the velocities of $\pm 5.67 \times 10^{-6}$ m/s for gaining and losing conditions in the y-direction corresponding to Fox et al. (2014), who applied velocities of ±49 cm/d at the bottom of the flume for losing and gaining conditions. A

fixed pressure of 0 Pa is defined at the outlet. For the gaining and losing conditions, the pressure at the bottom of the sediment is set to "fixedFluxPressure" to adjust the pressure gradient according to the fluxes at the boundary.

To quickly reach the quasi-steady state, adequate initial conditions are specified in analogy to measurements of Fox et al. (2014). The surface water velocity was set to 0.123 m/s in x-direction and the pore water velocity at the bottom of the sediment domain was set to 0 m/s for neutral conditions and to $\pm 5.67 \times 10^{-6}$ m/s in the y-direction for the gaining and losing cases. Since there is exchange across the sediment–water interface the values are only valid for the lower boundary of the sediment.

All cases run for 5 min without a tracer to approach steady state condition. Afterwards, a tracer with a molecular diffusion coefficient D_{mol} of 10^{-9} m^2/s enters with a concentration of 1 from the inlet into the domain. For gaining and losing conditions the incoming concentration at the bottom of the sediment is fixed to 0.

Results and Discussion

In the following we investigate the spreading of a conservative tracer with the novel integral modeling approach and compare the results with experimental observations of Fox et al. (2014) who used the dye tracer Brilliant Blue FCF to visualize the penetration of surface water into the sediment. For the comparison we use photo series of three experiments—that is, neutral, losing, and gaining condition. The photographs were taken every minute through the flume's glass walls. We compare photographs after every 10 min for the first hour of each experiment. The dyed area for the simulations as well as for the experiments were calculated using the software "ImageJ" for scientific image analysis and can be seen in Table 1. A threshold adjustment for RGB colors is applied to calculate the pixel area coverage. The propagation speeds of the tracer fronts in the sediments show a reasonable agreement (see Table 1). Next to the comparison of the tracer transport, we provide a closer understanding of the prevailing processes within the hyporheic zone through calculated velocity and pressure distributions.

Neutral Conditions

For neutral conditions, an impermeable wall is set at the bottom of the sediment. For all of our investigations we focused on the ripple in the middle of the flume (Figure 1). However, the flow processes are similar for all ripples (except for the first and the last ripple) as it can be seen in Figure 5a. Higher velocities within the surface water are observed above the ripple crests while lower velocities occur in the troughs. Within the sediment, the highest velocities can be seen at a small layer directly at the interface between the stream and the sediment as well as at the ripple crest (Figure 5b). The maximum Reynolds number in the sediment is 3.84, which means that Darcy's law is applicable.

Figure 5c shows the pressure distribution at the interface of surface and subsurface flow at the investigated ripple. The applied solver uses a specific formulation for the pressure where the pressure term p_rgh is used to avoid the occurrence of steep pressure gradients caused by hydrostatic effects. p_rgh is defined as the static pressure minus the hydrostatic pressure ($p_{rgh} = p - \rho g y$ with y as coordinate vector). The highest pressure is observed upstream of the crest. Lower pressure is determined downstream of the crest. Accordingly, the main flow within the sediment is from upstream of the crest to downstream—from high to low pressure. Additional flow occurs at the last third of the investigated ripple's lee face (Figure 5a and 5b). Consequently, two "hyporheic flow cells" with paths downwelling from surface water and returning to the water column within relatively short distances (Hester et al. 2013) are recognized for the neutral case at each ripple as also shown in three dimensions by Trauth et al. (2013) for pool riffle morphologies and earlier by Cardenas and Wilson (2007a) for ripples.

The two flow cells can also be seen in the tracer concentrations even though the second zone is still very thin after 1 h and hardly visible (Figure 6). Figure 6 shows the simulated tracer concentrations at the investigated ripple as well as the observed tracer spreading during the laboratory experiment for the first hour. A good agreement can be recognized with a root mean square error of 2.76 cm^2 (see Table 1), though a slightly faster spreading is observed within the simulations. A reason for this might be the shortened flume for the CFD simulation compared to the original flume length. Another reason might be that in the simulation the spread toward the edge of the plume can be seen with high-resolution results, while in the experiment lower concentrations are not visible in the pictures. Moreover, laboratory experiments cannot guarantee absolutely homogeneous sediment, which is assumed for our simulations. This means, that for example the grain size, the bulk density, and consequently also the porosity of the sediment can vary slightly and/or small deviations of neighboring ripple geometries can occur during the installation or during the experiment. Small-scale inhomogeneities can also be seen in the photographs, which show a slightly uneven course in the lower area of the tracer penetration. Since the simulation was only based on photos of the investigated ripple, all neighboring ripples are considered to have exactly the same geometry as the investigated ripple in our simulations.

Losing Conditions

The outflowing velocity at the bottom of the sediment is 5.67×10^{-6} m/s for losing conditions, which corresponds to the bottom flux used in the experiment by Fox et al. (2014).Compared to the neutral case the velocity distribution in the sediment changes drastically even though the surface water velocity is the same (compare Figures 5 and 7). The main flow direction within the sediment is downwards which can also be seen in the pressure distribution: low pressure occurs not only at and downstream

Table 1
Comparison of Dyed Areas for the Experiments and the Simulations at the Investigated Ripple Calculated with an Image Analysis Software

	Neutral		Losing		Gaining	
	Experiment	Simulation	Experiment	Simulation	Experiment	Simulation
10 min	6.163	6.685	21.732	20.082	4.083	4.011
30 min	20.654	20.705	51.105	51.900	7.765	7.861
60 min	27.695	32.439	85.483	90.691	9.906	9.888
Root mean square error	2.76		3.19		0.07	

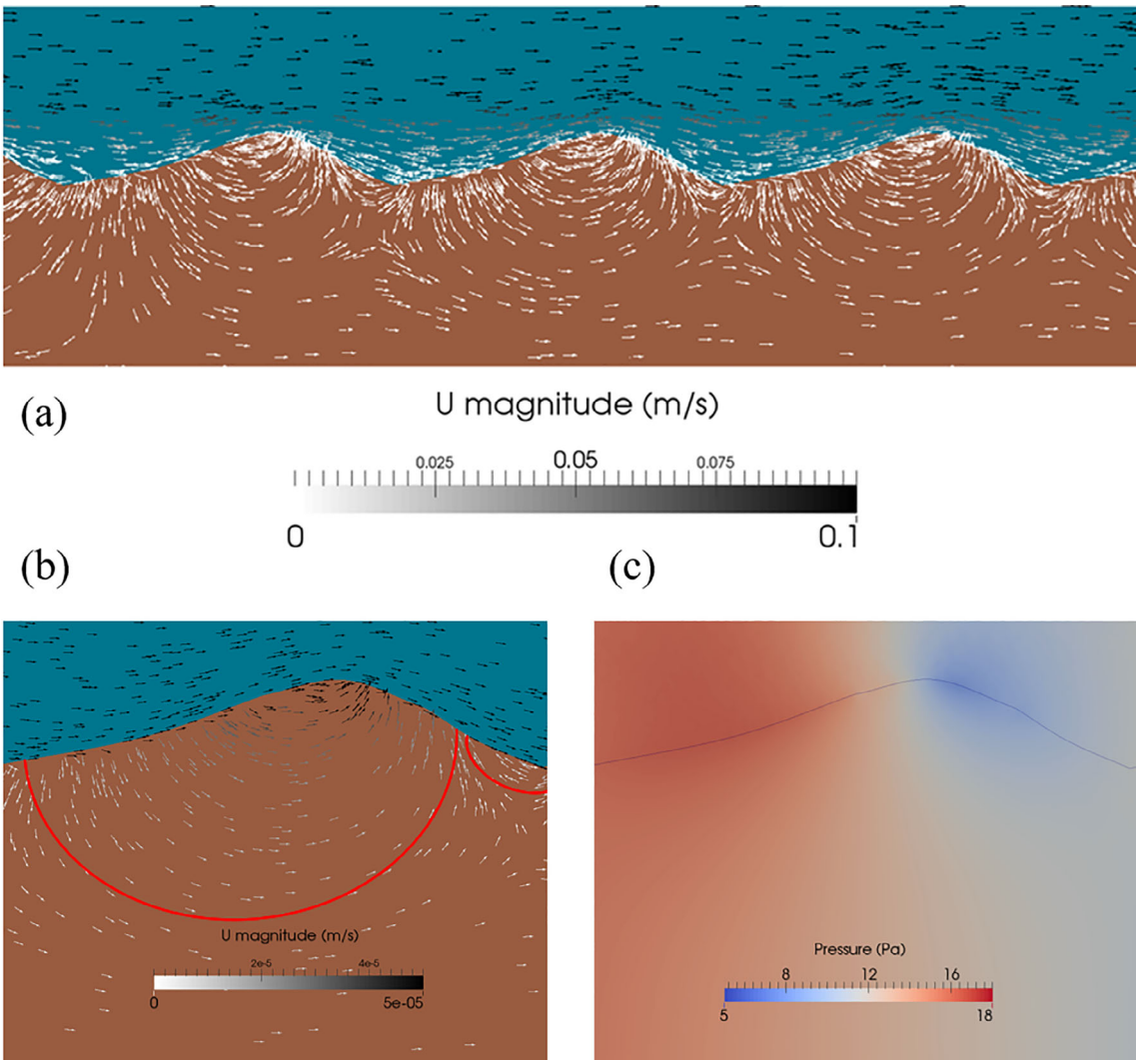

Figure 5. Velocity distribution of the neutral case at the rippled sediment (a) and velocity (b) and pressure distribution (c) at the investigated ripple. The red lines indicate the hyporheic flow cells.

of the ripple crest, but also toward the bottom of the sediment (Figure 7c). Still most of the surface water that enters the sediment flows into the ripple at the stoss side, where the highest pressure is observed (Figure 7b and 7c). However, a further fraction comes from the last third of the lee side of the ripple and flows (except of a small layer at the interface to the surface water) in upstream direction. These different flow cells that are pointing in upstream as well as in downstream directions for infiltrating stream water were also observed in several studies investigating losing conditions (Cardenas and Wilson 2007b; Boano et al. 2008; Trauth et al. 2013).

The flow entering the ripple is divided into a part that gets back to the surface water and another part that flows toward the bottom of the sediment domain. Hyporheic exchange flow, that is, flow paths beginning and ending at

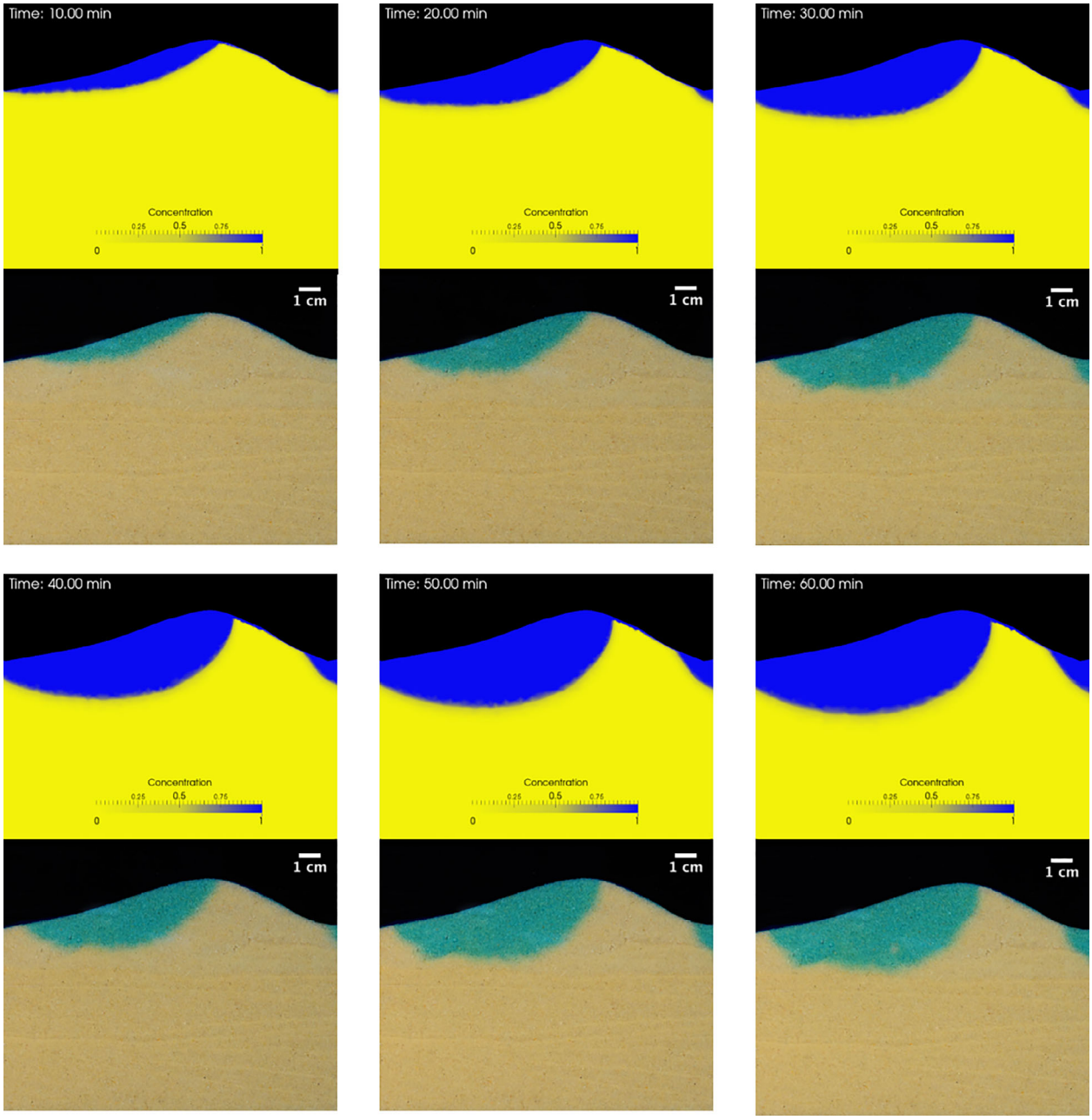

Figure 6. Simulated tracer concentrations (yellow blue images) and photos of laboratory experiments (beige-turquoise) after Fox et al. (2014) for 10–60 min under neutral conditions.

the sediment–water interface, is centered around the ripple crest and at a shallow area at the lee side. Compared to neutral conditions, a larger area with high velocities is observed in the sediment—especially around the ripple crest, but also at the stoss side (compare Figures 5b and 7b) which was also seen in Trauth et al. (2013). For losing conditions in this case the Reynolds numbers increase slightly with a maximum of 4.23 compared to the neutral conditions. However, the Darcy law is still applicable. Cardenas and Wilson (2007c) stated that large temperature variations of the water column penetrate deep into the subsurface for losing conditions and that with increasing downwelling the temperature signal penetrates deeper into the sediment—especially at the stoss side of ripples and at a narrow upwelling zone below the crest. These observations coincide qualitatively with our simulation and the observations by Fox et al. (2014).

Figure 8 shows the tracer spreading for losing conditions during the flume experiment compared with simulated tracer concentrations. In the first 20 min the tracer concentrations downstream of the ripple crest are slightly lower for the simulations compared to the photos of the experiment. This can be based on small variations of the sediment parameters during the experiments or due to slight variations of the ripple geometry from the simulations compared to the experiment. Moreover, the ripple geometries of the neighboring ripples can influence

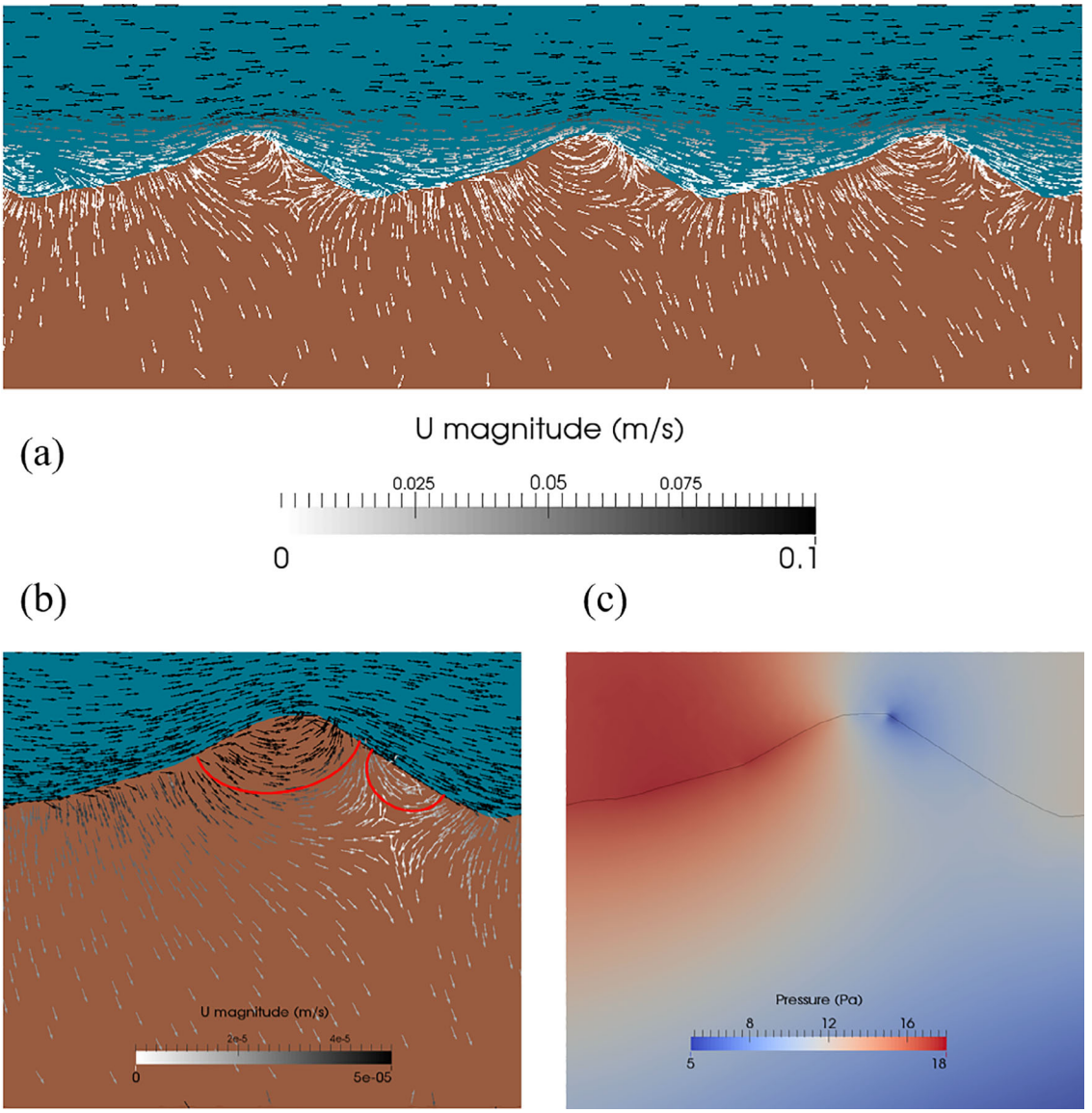

Figure 7. Velocity distribution for losing conditions at the rippled sediment (a) and velocity (b) and pressure distribution (c) at the investigated ripple. The red lines indicate the hyporheic flow cells.

the spreading. But overall, a good agreement between the experimental observations and the simulations is observed with a root mean square error of 3.19 cm^2. Especially the most important structures of losing conditions compared to neutral and gaining conditions can be well recognized. Due to the higher velocities in the sediment under losing conditions compared to neutral conditions (Figure 7b) the tracer penetrates much faster into the sediment compared to neutral conditions (Figure 6). Moreover, in the velocity field we can see that the surface water infiltrates almost at the whole lee side of the ripple directly into the sediment, while under neutral conditions the tracer flows in upstream direction and colors the ripple toe only through hyporheic exchange. Under neutral conditions the tracer flows into the ripple and then back to the surface water; under losing conditions most of the tracer mass that enters the ripple flows toward the bottom of the model (Figure 7a). Therefore, the infiltrated area increases constantly during the experiment (and consequently also during the simulation).

Gaining Conditions

For gaining conditions we use the same flow velocity at the bottom of the sediment domain as for losing conditions but in opposite direction. Accordingly, the flow field within the sediment changes from downward to upward (Figure 9a and 9b). Surface water enters the sediment only at the stoss side of ripples which is consistent with Trauth et al. (2013). Cardenas and Wilson (2007b) also stated that the geometry of hyporheic flow cells is different for gaining and losing conditions even if the depth of the hyporheic flow cells is similar for gaining and losing condition. Hyporheic exchange flow, that is, flow paths beginning and ending at the sediment–water interface, is centered at the stoss side of ripples for gaining condition. In contrast to

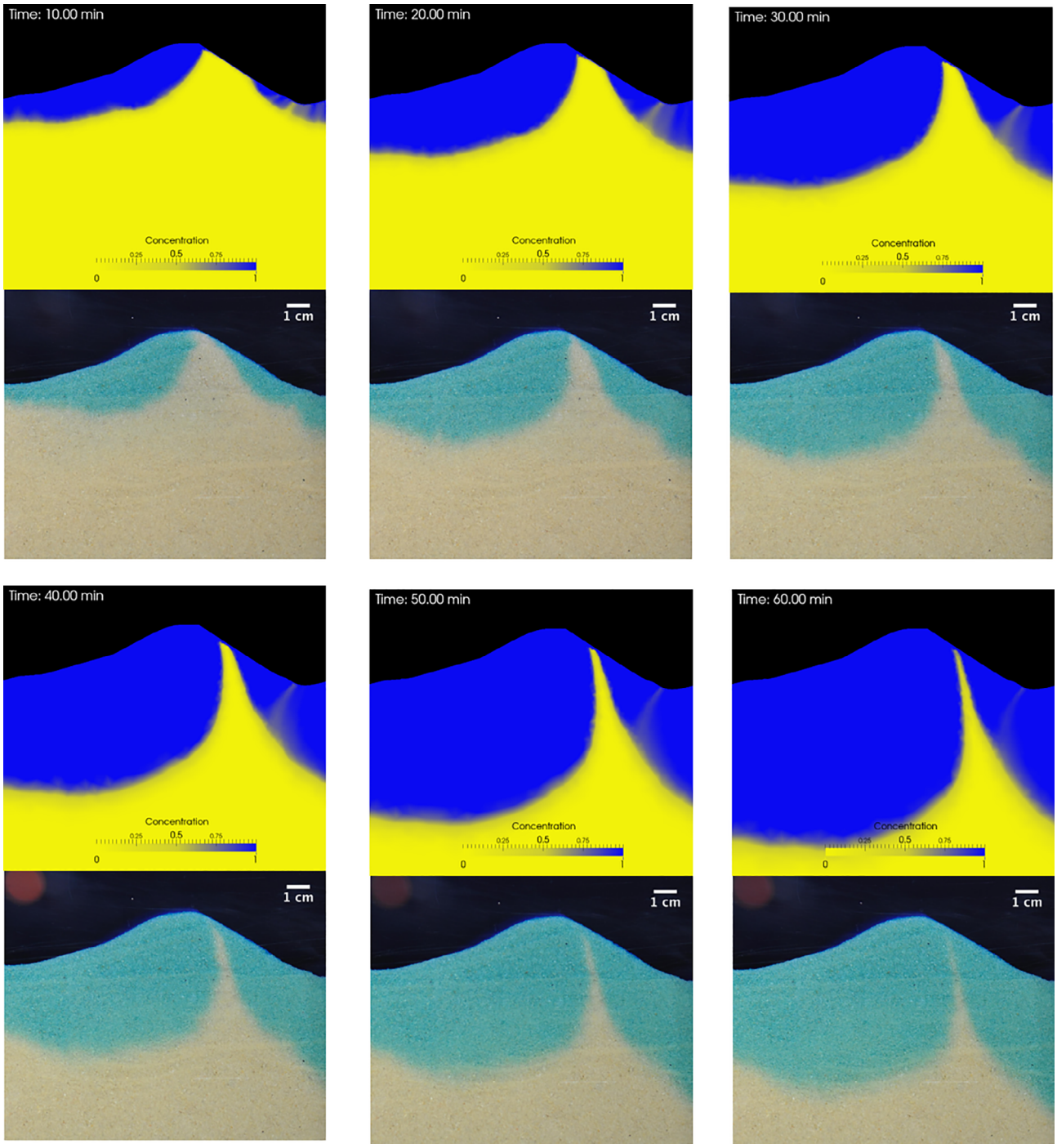

Figure 8. Simulated tracer concentrations (yellow blue images) and photos of laboratory experiments (beige-turquoise) after Fox et al. (2014) for 10–60 min under losing conditions.

neutral and losing conditions, under gaining conditions outflowing subsurface flow is not only observed at the lee side of the ripple but also at the beginning of the stoss side (Figure 9b). Trauth et al. (2013) observed upstream and downstream directed hyporheic flow cells for gaining conditions. In the present modeling study upstream directed flow originates from deeper pore water (groundwater) while hyporheic exchange flow is only directed downstream. As also indicated by the pressure field (Figure 9c) and velocity distribution (Figure 9a and 9b), flow occurs from high pressure in the first section of the stoss side of the ripple toward the second section of the stoss side and from the high pressure zone at the bottom of the sediment domain to the low pressure zone at the lee side of the ripple. The same main flow directions for gaining conditions were also observed by Cardenas and Wilson (2007b).

Comparing the hyporheic flow fields of gaining and losing conditions, we conclude that faster hyporheic flow and thus shorter residence times occur under losing

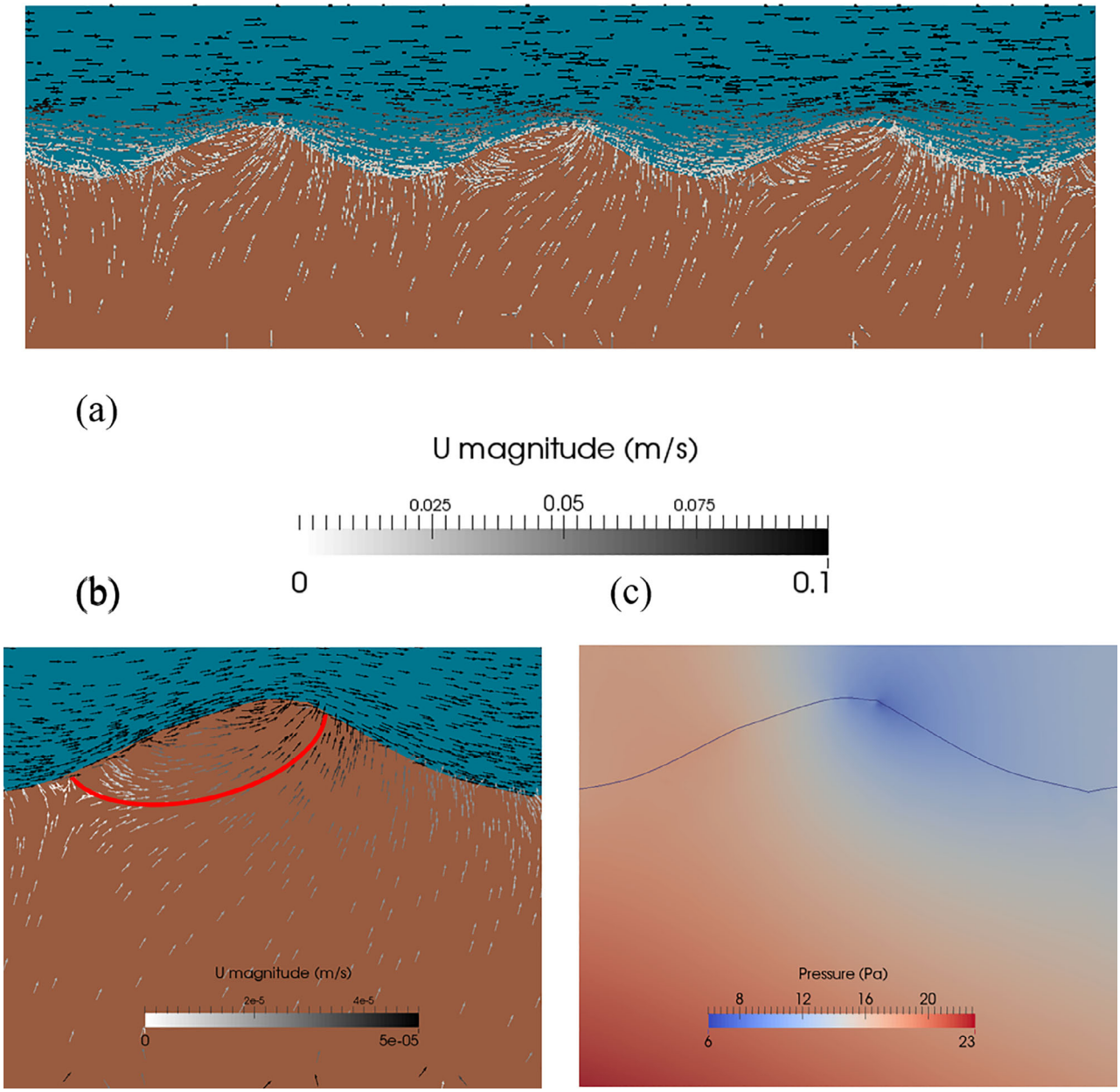

Figure 9. Velocity distribution for gaining conditions at the rippled sediment (a) and velocity (b) and pressure distribution (c) at the investigated ripple. The red line indicates the hyporheic flow cell.

conditions. This supports results of Trauth et al. (2013). Shorter residence times can significantly affect biogeochemical processes (Zarnetske et al. 2011).

In contrast to neutral and losing conditions, only one hyporheic flow cell occurs under gaining conditions. This single flow cell is also reflected in the transport of the dye tracer (Figure 10). Moreover, there is less tracer mass transported into the sediment compared to neutral and losing conditions due to the upward directed flow of the groundwater (compare Figures 6, 8, and 10). This was also seen in Fox et al. (2014) and there is a good agreement between their laboratory observations and the modeled tracer concentrations of the present study with a root mean square error of 0.07 cm^2. Even after 4 h, the tracer spreading observed by Fox et al. (2014) did not vary much since the colored area is only caused by hyporheic flow cells.

Conceptual and Computational Consideration

Regarding the general application of Computational Fluid Dynamics software, we want to point out, that a lot of decisions have to be made to find the right model for each investigation. The user can, for example, decide whether water level fluctuations are important and thus a two-phase model has to be chosen or if a one phase model is sufficient. Also, it has to be decided whether one-, two-, or three dimensions are investigated. These decisions affect the quality of the results as well as the computational effort and depend on the aim of the investigation. Also, the boundary and

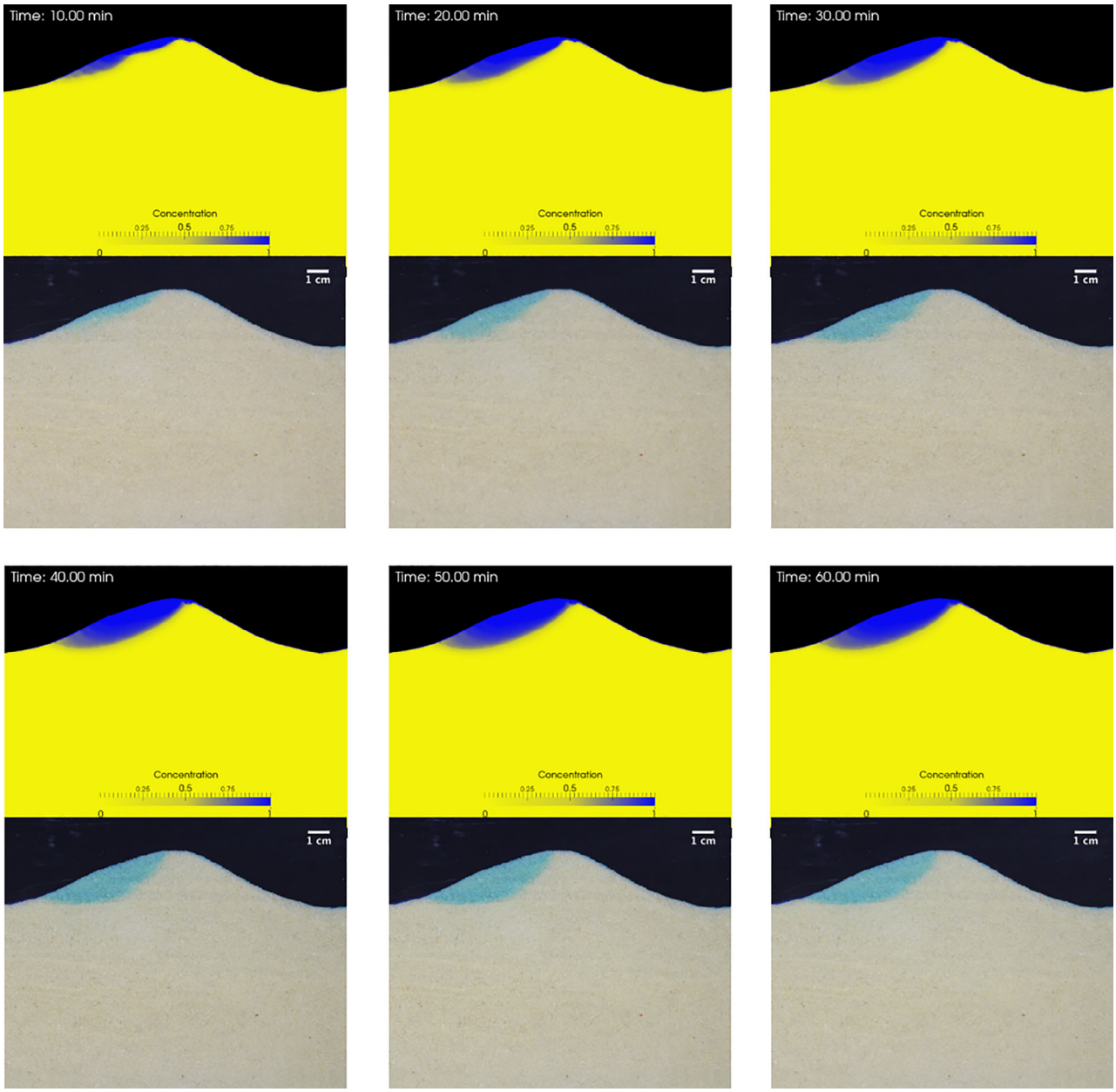

Figure 10. Simulated tracer concentrations (yellow blue images) and photos of laboratory experiments (beige-turquoise) after Fox et al. (2014) for 10–60 min under gaining conditions.

initial conditions as well as the mesh quality influence the results significantly. As a consequence, even though we do not have one or various parameters to calibrate, it is not always easy to find the right model settings. These points are independent of the presented integral modeling approach and are also applicable for other CFD approaches. As mentioned in the introduction, various studies investigated flow and transport processes in the hyporheic zone using coupled modeling approaches. In the present study, we present and validate an integral model which has some advantages and disadvantages compared to the coupled approaches. For the coupled approaches usually a surface water model is applied and subsequently the corresponding pressure distribution is used as an input for the calculation with a groundwater model. Commonly, different time steps are used for the groundwater and the surface water model in the coupled approach while for the integral model the time step is the same for the whole model domain. On the one hand, a direct feedback from the subsurface to the surface and vice versa is possible for every time step in the coupled approach. On the other hand, a high computational effort is needed. The direct feedback can be important, for example, for unsteady flow conditions, which can have a significant impact on biogeochemical processes in the hyporheic zone (Galloway et al. 2019). In contrast to coupled approaches, variations of velocity or tracer concentration within both surface water and sediment and their effects on flow and transport processes can be directly observed at the same time in the whole domain with the integral model.

Especially compared to one-way sequentially coupled approaches the integral approach is more appropriate if, for example, a contamination of the groundwater that spreads into the surface water is considered.

Also turbulent structures that can penetrate from the surface water into the sediment can be simulated, which is not possible with coupled approaches that use the Darcy law to describe flow processes within the sediment. An accurate description of all turbulent structures is only possible by directly resolving them (i.e. using DNS approaches). But facing the computational effort, we decided to use a RANS turbulence model for this study as the turbulent structures can still be depicted qualitatively well. The k-epsilon turbulence model was applied as it showed better results than the k-omega model, used, for example, by Cardenas and Wilson (2007b, 2007c). This is probably based on the fact that we did not set a wall at the interface of surface and subsurface water in contrast to Cardenas and Wilson (2007b, 2007c). The k-omega turbulence model has the advantage compared to the k-epsilon model to show better results close to walls. Also three-dimensional investigations using advanced turbulence models such as LES are generally possible with the integral solver as applied by Broecker et al. (2019). However, this turbulence model causes again considerably more computational effort.

In the present study, we validated the new integral model for transport processes at the hyporheic zone with previously performed flume experiments. Compared to one-way coupled approaches the integral model is definitely more time consuming. However, the integral solver is applicable where commonly used coupled approaches cannot be applied as, for example, for Reynolds numbers higher than 10 and where the Darcy law would consequently lead to overestimated flow rates. In the present study the maximum Reynolds number was lower than 5 which means that a coupled model has probably similar results. But Broecker et al. (2019) showed that already coarser sand can lead to significantly higher Reynolds numbers in the sediment close to the interface. For these sediments with bigger grain sizes which lead to non-Darcy flow areas, the integral model is still applicable and additionally the calculation time is considerably smaller than for fine sediments.

Conclusions

In this study we present and validate an integral solver which was extended for tracer transport at the interface of surface water and groundwater. Similar observations were stated in previously presented modeling approaches that coupled a surface water model with a groundwater model. However, the integral model can also be used for unsteady conditions in groundwater or surface water and can show direct feedbacks from the surface water to the groundwater and vice versa. It is also applicable in non-Darcy flow layers as an extended version of the Navier–Stokes equations is solved in the stream as well as in the sediment, which is especially important for bigger grain sizes.

The results demonstrate the reliability of our modeling study and provide further insights into a laboratory experiment for the transport of a dye tracer. With the integral solver it is possible to depict complex hydraulics and their effects on tracer transport at the interface of groundwater and the stream. Results like the thin top layer for the neutral case with inflowing surface water on the lee side (depicted within the simulations as well as during the experiments) would look completely different with a one-way coupled model. A detailed comparison between one way coupled and the integral model is planned. In future, the integral solver can also be applied to heterogeneous sediments (with different grain size diameters and porosities) but a validation for heterogeneous sediments is still needed. As a basis for the validation of the integral model for heterogeneous sediments, a further experiment of Fox et al. (2016) conducted in the same flume system but with different sediment can be used. For examinations over long periods of time or for larger investigation areas upscaling methods are required.

Acknowledgments

We would like to acknowledge the time and effort by Jan H. Fleckenstein to improve the quality of this paper. The funding provided by the German Research Foundation (DFG) within the Research Training Group "Urban Water Interfaces" (GRK 2032) and the grant from the Technische Universität Berlin, Germany, are gratefully acknowledged. Data archiving for all simulations and analytical results are underway and will be available in the repository of the Technische Universität Berlin "DepositOnce." Datasets of the experimental results used for this research are included in this paper. Open access funding enabled and organized by ProjektDEAL.

Authors' Note

The authors do not have any conflicts of interest or financial disclosures to report.

References

Alaghmand, S., S. Beecham, I.D. Jolly, K.L. Holland, J.A. Woods, and A. Hassanli. 2014. Modelling the impacts of river stage manipulation on a complex river-floodplain system in a semi-arid region. *Environmental Modelling & Software* 59: 109–126.

Arnon, S., K. Yanuka, and A. Nejidat. 2013. Impact of overlying water velocity on ammonium uptake by benthic biofilms. *Hydrological Processes* 27, no. 4: 570–578.

Bardini, L., F. Boano, M.B. Cardenas, R. Revelli, and L. Ridolfi. 2012. Nutrient cycling in bedform induced hyporheic zones. *Geochimica et Cosmochimica Acta* 84: 47–61.

Bencala, K.E., and R.A. Walters. 1983. Simulation of solute transport in a mountain pool-and-riffle stream: A transient storage model. *Water Resources Research* 19, no. 3: 718–724.

Boano, F., R. Revelli, and L. Ridolfi. 2008. Reduction of the hyporheic zone volume due to the stream-aquifer interaction. *Geophysical Research Letters* 35, no. 9. http://dx.doi.org/10.1029/2008gl033554.

Botter, G., N.B. Basu, S. Zanardo, P.S.C. Rao, and A. Rinaldo. 2010. Stochastic modeling of nutrient losses in streams: Interactions of climatic, hydrologic and biogeochemical controls. *Water Resources Research* 46, no. 8.

Boulton, A., T. Datry, T. Kasahara, M. Mutz, and J. Stanford. 2010. Ecology and management of the hyporheic zone: Stream-groundwater interactions of running waters and their floodplains. *Journal of the North American Benthological Society* 29: 26–40.

Broecker, T., K. Teuber, V. Sobhi Gollo, G. Nützmann, J. Lewandowski, and R. Hinkelmann. 2019. Integral flow modelling approach for surface water-groundwater interactions along a rippled streambed. *Water* 11, no. 7: 1517.

Brunke, M., and T. Gonser. 1997. The ecological significance of exchange processes between rivers and groundwater. *Freshwater Biology* 37, no. 1: 1–33.

Brunner, P., and C.T. Simmons. 2012. HydroGeoSphere: A fully integrated, physically based hydrological model. *Groundwater* 50, no. 2: 170–176.

Brunner, P., P.G. Cook, and C.T. Simmons. 2009. Hydrogeologic controls on disconnection between surface water and groundwater. *Water Resources Research* 45, no. 1.

Buffington, J.M., and D. Tonina. 2009. Hyporheic exchange in mountain rivers II: Effects of channel morphology on mechanics, scales, and rates of exchange. *Geography Compass* 3, no. 3: 1038–1062.

Burnett, W.C., H. Bokuniewicz, M. Huettel, W.S. Moore, and M. Taniguchi. 2003. Groundwater and pore water inputs to the coastal zone. *Biogeochemistry* 66, no. 1: 3–33.

Cardenas, M.B. 2009. Stream-aquifer interactions and hyporheic exchange in gaining and losing sinuous streams. *Water Resources Research* 45, no. 6.

Cardenas, M.B., and J.L. Wilson. 2007a. Dunes, turbulent eddies, and interfacial exchange with permeable sediments. *Water Resources Research* 43, no. 8.

Cardenas, M.B., and J.L. Wilson. 2007b. Exchange across a sediment–water interface with ambient groundwater discharge. *Journal of Hydrology* 346: 69–80.

Cardenas, M.B., and J.L. Wilson. 2007c. Thermal regime of dune-covered sediments under gaining and losing water bodies. *Journal of Geophysical Research: Biogeosciences* 112, no. G4. http://dx.doi.org/10.1029/2007jg000485.

Cheng, N.-S., and Y.-M. Chiew. 1998. Modified logarithmic law for velocity distribution subjected to upward seepage. *Journal of Hydraulic Engineering* 124, no. 12: 1235–1241.

Dent, C.L., N.B. Grimm, E. Martí, J.W. Edmonds, J.C. Henry, and J.R. Welter. 2007. Variability in surface-subsurface hydrologic interactions and implications for nutrient retention in an arid-land stream. *Journal of Geophysical Research: Biogeosciences* 112, no. G4. http://dx.doi.org/10.1029/2007jg000467

Elliott, A.H., and N.H. Brooks. 1997. Transfer of nonsorbing solutes to a streambed with bed forms: Laboratory experiments. *Water Resources Research* 33, no. 1: 137–151.

Engelhardt, I., J.A.C. Barth, R. Bol, M. Schulz, T.A. Ternes, C. Schüth, and R. van Geldern. 2014. Quantification of long-term wastewater fluxes at the surface water/groundwater-interface: An integrative model perspective using stable isotopes and acesulfame. *Science of the Total Environment* 466–467: 16–25.

Ergun, S. 1952. Fluid flow through packed column. *Chemical Engineering Progress* 48: 89–94.

Fox, A., G. Laube, C. Schmidt, J.H. Fleckenstein, and S. Arnon. 2016. The effect of losing and gaining flow conditions on hyporheic exchange in heterogeneous streambeds. *Water Resources Research* 52, no. 9: 7460–7477.

Fox, A., F. Boano, and S. Arnon. 2014. Impact of losing and gaining streamflow conditions on hyporheic exchange fluxes induced by dune-shaped bed forms. *Water Resources Research* 50, no. 3: 1895–1907.

Galloway, J., A. Fox, J. Lewandowski, and S. Arnon. 2019. The effect of unsteady streamflow and stream-groundwater interactions on oxygen consumption in a sandy streambed. *Scientific Reports* 9, no. 1: 19735.

Gariglio, F.P., D. Tonina, and C.H. Luce. 2013. Spatiotemporal variability of hyporheic exchange through a pool-riffle-pool sequence. *Water Resources Research* 49, no. 11: 7185–7204.

Geuzaine, C., and J.-F. Remacle. 2009. Gmsh: A 3-D finite element mesh generator with built-in pre- and post-processing facilities. *International Journal for Numerical Methods in Engineering* 79, no. 11: 1309–1331.

Gomez, J.D., J.L. Wilson, and M.B. Cardenas. 2012. Residence time distributions in sinuosity-driven hyporheic zones and their biogeochemical effects. *Water Resources Research* 48, no. 9. http://dx.doi.org/10.1029/2012wr012180.

Harvey, J.W., J.K. Böhlke, M.A. Voytek, D. Scott, and C.R. Tobias. 2013. Hyporheic zone denitrification: Controls on effective reaction depth and contribution to whole-stream mass balance. *Water Resources Research* 49, no. 10: 6298–6316.

Harvey, J.W., and K.E. Bencala. 1993. The effect of streambed topography on surface-subsurface water exchange in mountain catchments. *Water Resources Research* 29, no. 1: 89–98.

Heberer, T., G. Massmann, B. Fanck, T. Taute, and U. Duennbier. 2008. Behaviour and redox sensitivity of antimicrobial residues during bank filtration. *Chemosphere* 73: 451–460.

Hester, E.T., K.I. Young, and M.A. Widdowson. 2013. Mixing of surface and groundwater induced by riverbed dunes: Implications for hyporheic zone definitions and pollutant reactions. *Water Resources Research* 49, no. 9: 5221–5237.

Hester, E.T., and M.N. Gooseff. 2010. Moving beyond the banks: Hyporheic restoration is fundamental to restoring ecological services and functions of streams. *Environmental Science & Technology* 44, no. 5: 1521–1525.

Huettel, M., H. Røy, E. Precht, and S. Ehrenhauss. 2003. Hydrodynamical impact on biogeochemical processes in aquatic sediments: The interactions between sediments and water (Guest Editor: Brian Kronvang). *Hydrobiologia* 494: 231–236.

Huntscha, S., H. Singer, C. McArdell, C. Frank, and J. Hollender. 2012. Multiresidue analysis of 88 polar organic micropollutants in ground, surface and wastewater using online mixed-bed multilayer solid-phase extraction coupled to high performance liquid chromatography-tandem mass spectrometry. *Journal of Chromatography. A* 1268: 74–83.

Jin, G., H. Tang, L. Li, and D.A. Barry. 2011. Hyporheic flow under periodic bed forms influenced by low-density gradients. *Geophysical Research Letters* 38, no. 22. http://dx.doi.org/10.1029/2011gl049694

Jones, J.B., and P.J. Mulholland. 2000. *Streams and Ground Waters*. San Diego, California: Academic Press.

Kasahara, T., and S.M. Wondzell. 2003. Geomorphic controls on hyporheic exchange flow in mountain streams. *Water Resources Research* 39, no. 1: SBH 3-1–SBH 3-14.

Kinzelbach, W. 1992. *Numerische Methoden zur Modellierung des Transports von Schadstoffen im Grundwasser*. Munich, Germany: Oldenbourg Wissenschaftsverlag.

Krause, S., C. Tecklenburg, M. Munz, and E. Naden. 2013. Streambed nitrogen cycling beyond the hyporheic zone: Flow controls on horizontal patterns and depth distribution of nitrate and dissolved oxygen in the upwelling groundwater of a lowland river. *Journal of Geophysical Research: Biogeosciences* 118, no. 1: 54–67.

Lawrence, J., M. Skold, F. Hussain, D. Silverman, V. Resh, D. Sedlak, R. Luthy, and J. McCray. 2013. Hyporheic

zone in urban streams: A review and opportunities for enhancing water quality and improving aquatic habitat by active management. *Environmental Engineering Science* 30: 480–501.

Lewandowski, J., S. Arnon, E. Banks, O. Batelaan, A. Betterle, T. Broecker, C. Coll, J.D. Drummond, J. Gaona Garcia, J. Galloway, J. Gomez-Velez, R.C. Grabowski, S.P. Herzog, R. Hinkelmann, A. Höhne, J. Hollender, M.A. Horn, A. Jaeger, S. Krause, A. Löchner Prats, C. Magliozzi, K. Meinikmann, B.B. Mojarrad, B.M. Mueller, I. Peralta-Maraver, A.L. Popp, M. Posselt, A. Putschew, M. Radke, M. Raza, J. Riml, A. Robertson, C. Rutere, J.L. Schaper, M. Schirmer, H. Schulz, M. Shanafield, T. Singh, A.S. Ward, P. Wolke, A. Wörman, and L. Wu. 2019. Is the hyporheic zone relevant beyond the scientific community? *Water* 11, no. 11: 2230.

Lewandowski, J., L. Angermann, G. Nützmann, and J.H. Fleckenstein. 2011a. A heat pulse technique for the determination of small-scale flow directions and flow velocities in the streambed of sand-bed streams. *Hydrological Processes* 25, no. 20: 3244–3255.

Lewandowski, J., A. Putschew, D. Schwesig, C. Neumann, and M. Radke. 2011b. Fate of organic micropollutants in the hyporheic zone of a eutrophic lowland stream: Results of a preliminary field study. *The Science of the Total Environment* 409, no. 10: 1824–1835.

Li, B., X. Liu, M.H. Kaufman, A. Turetcaia, X. Chen, and M.B. Cardenas. 2020. Flexible and modular simultaneous modeling of flow and reactive transport in rivers and hyporheic zones. *Water Resources Research* 56, no. 2: e2019WR026528.

Marzadri, A., D. Tonina, and A. Bellin. 2012. Morphodynamic controls on redox conditions and on nitrogen dynamics within the hyporheic zone: Application to gravel bed rivers with alternate-bar morphology. *Journal of Geophysical Research: Biogeosciences* 117, no. G3. http://dx.doi.org/10.1029/2012jg001966.

Mermillod-Blondin, F., M. Creuze des Chatelliers, P. Marmonier, and M.-J. Dole-Olivier. 2000. Distribution of solutes, microbes and invertebrates in river sediments along a riffle-pool-riffle sequence. *Freshwater Biology* 44, no. 2: 255–269.

Nützmann, G., and S. Mey. 2007. Model-based estimation of runoff changes in a small lowland watershed of north-eastern Germany. *Journal of Hydrology* 334, no. 3: 467–476.

Oxtoby, O., J. Heyns, and R. Suliman. 2013. A finite-volume solver for two-fluid flow in heterogeneous porous media based on OpenFOAM. Paper presented at Open Source CFD International Conference, Hamburg, Germany.

Packman, A.I., M. Salehin, and M. Zaramella. 2004. Hyporheic exchange with gravel beds: Basic hydrodynamic interactions and bedform-induced advective flows. *Journal of Hydraulic Engineering* 130, no. 7: 647–656.

Peterson, E.W., and T.B. Sickbert. 2006. Stream water bypass through a meander neck, laterally extending the hyporheic zone. *Hydrogeology Journal* 14, no. 8: 1443–1451.

Prinos, P. 1995. Bed-suction effects on structure of turbulent open-channel flow. *Journal of Hydraulic Engineering* 121, no. 5: 404–412. http://dx.doi.org/10.1061/(asce)0733-9429(1995)121:5(404).

Regnery, J., J. Barringer, A. Wing, C. Hoppe-Jones, J. Teerlink, and J. Drewes. 2015. Start-up performance of a full-scale riverbank filtration site regarding removal of DOC, nutrients, and trace organic chemicals. *Chemosphere* 127C: 136–142.

Roche, K.R., G. Blois, J.L. Best, K.T. Christensen, A.F. Aubeneau, and A.I. Packman. 2018. Turbulence links momentum and solute exchange in coarse-grained streambeds. *Water Resources Research* 54, no. 5: 3225–3242.

Ruehl, C., A. Fisher, M. Los Huertos, S. Wankel, C. Wheat, C. Kendall, C. Hatch, and C. Shennan. 2009. Nitrate dynamics within the Pajaro River, a nutrient-rich, losing stream. *Journal of the North American Benthological Society* 26: 191–206.

Schaper, J.L., M. Posselt, C. Bouchez, A. Jaeger, G. Nuetzmann, A. Putschew, G. Singer, and J. Lewandowski. 2019. Fate of trace organic compounds in the hyporheic zone: Influence of retardation, the benthic biolayer, and organic carbon. *Environmental Science & Technology* 53, no. 8: 4224–4234.

Schaper, J.L., M. Posselt, J.L. McCallum, E.W. Banks, A. Hoehne, K. Meinikmann, M.A. Shanafield, O. Batelaan, and J. Lewandowski. 2018. Hyporheic exchange controls fate of trace organic compounds in an urban stream. *Environmental Science & Technology* 52, no. 21: 12285–12294.

Sophocleous, M. 2002. Interactions between groundwater and surface water: The state of the science. *Hydrogeology Journal* 10, no. 1: 52–67.

Stofleth, J.M., F.D. Shields Jr.., and G.A. Fox. 2008. Hyporheic and total transient storage in small, sand-bed streams. *Hydrological Processes* 22, no. 12: 1885–1894.

Tonina, D., and J.M. Buffington. 2007. Hyporheic exchange in gravel bed rivers with pool-riffle morphology: Laboratory experiments and three-dimensional modeling. *Water Resources Research* 43, no. 1. http://dx.doi.org/10.1029/2005wr004328.

Trauth, N., C. Schmidt, M. Vieweg, S.E. Oswald, and J.H. Fleckenstein. 2015. Hydraulic controls of in-stream gravel bar hyporheic exchange and reactions. *Water Resources Research* 51: 2243–2263.

Trauth, N., C. Schmidt, M. Vieweg, U. Maier, and J.H. Fleckenstein. 2014. Hyporheic transport and biogeochemical reactions in pool-riffle systems under varying ambient groundwater flow conditions. *Journal of Geophysical Research: Biogeosciences* 119, no. 5: 910–928.

Trauth, N., C. Schmidt, U. Maier, M. Vieweg, and J. Fleckenstein. 2013. Coupled 3-D stream flow and hyporheic flow model under varying stream and ambient groundwater flow conditions in a pool-riffle system. *Water Resources Research* 49, no. 9: 5834–5850.

van der Molen, D.T., A. Breeuwsma, and P.C.M. Boers. 1998. Agricultural nutrient losses to surface water in the Netherlands: Impact, strategies, and perspectives. *Journal of Environmental Quality* 27, no. 1: 4–11.

van Gent, M. 1995. *Wave Interaction with Permeable Coastal Structures*. Amsterdam, The Netherlands: Elsevier Science.

VanderKwaak, J.E. 1999. Numerical simulation of flow and chemical transport in integrated surface-subsurface hydrologic systems. PhD thesis, University of Waterloo, Waterloo, Canada.

Wu, L., T. Singh, J. Gomez-Velez, G. Nützmann, A. Wörman, S. Krause, and J. Lewandowski. 2018. Impact of dynamically changing discharge on hyporheic exchange processes under gaining and losing groundwater conditions. *Water Resources Research* 54, no. 12: 10076–10093.

Zarnetske, J.P., R. Haggerty, S.M. Wondzell, and M.A. Baker. 2011. Dynamics of nitrate production and removal as a function of residence time in the hyporheic zone. *Journal of Geophysical Research: Biogeosciences* 116, no. G1. http://dx.doi.org/10.1029/2010jg001356.